ACS Catalysis

Research Article

Cite This: ACS Catal. 2019, 9, 5567−5573

pubs.acs.org/acscatalysis

Theoretical Resolution of the Exceptional Oxygen Reduction Activity of Au(100) in Alkaline Media

Zhiyao Duan and Graeme Henkelman*

Department of Chemistry and the Oden Institute for Computational Engineering and Sciences, The University of Texas at Austin, Austin, Texas 78712-0165, United States

Supporting Information

ABSTRACT: The reason that Au(100) surfaces have exceptional activity toward the oxygen reduction reaction (ORR) in alkaline media has been a long-standing puzzle that remains unexplained. Theoretically, the high activity of Au(100) cannot be understood entirely by the widely employed computational hydrogen electrode method, because oxygen adsorption on Au(100) is calculated to be too weak. Here we present a density functional theory study of the electrochemical Au(100)/aqueous interface under constant potential conditions. Calculations of how the adsorption energies of the ORR intermediates vary as a function of applied potential and pH show that $*O_2H$ can be stabilized in alkaline media as compared to acidic media, leading to enhanced ORR activity. Adsorbed *OH can further stabilize $*O_2H$ adsorbed at a nearest neighbor site leading to the favorable $4e^-$ reduction pathway and an onset potential of 0.81 V vs the reversible hydrogen electrode. These results provide a direct comparison to experiments and insight into the influence of the electrochemical interface on the ORR energetics.

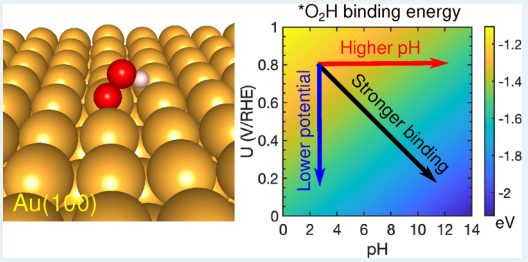

KEYWORDS: *oxygen reduction reaction, Au(100), alkaline media, density functional theory, constant potential condition, double reference method, implicit solvation*

INTRODUCTION

The oxygen reduction reaction (ORR) is an important reaction for electrochemical energy conversion devices, such as low temperature fuel cells. Platinum and its alloys are currently the most efficient catalysts for the ORR.[1,2] Their exceptional activity originates from the optimal adsorption energies of the oxygenated intermediates on the surfaces of these catalysts.[3] The adsorption energies of the oxygenated species should be strong enough to break the O−O bond for catalyzing the $4e^-$ ORR but not so strong that they poison the catalyst. Gold is normally considered an inactive catalyst for the $4e^-$ ORR because of weak adsorption on gold surfaces.[3] The ORR on gold has been studied extensively both in acidic and in alkaline solutions.[4−10] Consistent with theoretical predictions, in acidic solutions, a $2e^-$ pathway producing hydrogen peroxide is dominant for all Au surfaces studied. Surprisingly though, the Au(100) surface is not only active for $4e^-$ ORR but is even more active than Pt in alkaline media in a certain potential range.[11] This observation has puzzled scientists for decades and remains unexplained.

The ORR on Au(100) exhibits a strong pH dependence. For pH values below 6, the reduction of O_2 follows the $2e^-$ process. For pH values higher than 6, the $4e^-$ reduction process is active in the potential range where adsorbed OH^- anions are present.[7,8] The adsorption of OH^- has been found to be essential for $4e^-$ O_2 reduction because the potential region where the $4e^-$ ORR is active coincides with the presence of adsorbed OH^- at the surface.[8] Although these observations were made decades ago, a fundamental understanding of the relationship between OH^- adsorption and $4e^-$ ORR activity is not understood. Recently, using density functional theory (DFT), it was shown that coadsorbed water can promote O−O bond breaking and thus leads to $4e^-$ reduction.[12] These calculations, however, do not explain the pH-dependent ORR pathway and the critical role of adsorbed OH^-.

The computational hydrogen electrode (CHE) method, proposed by Nørskov and co-workers, has been successfully used to calculate the overpotential of the ORR on various catalytic surfaces.[3] We applied the method for the ORR on the Au(100) surface; the result is presented in Figure 1. The onset potential for the ORR on Au(100) is calculated to be 0.18 V vs the reversible hydrogen electrode (RHE), which corresponds to an overpotential of 1.05 V/RHE. In the CHE method, dependence on pH is corrected using the free energy of H^+ as kT ln(10)pH. Since the RHE accounts for pH, the calculated overpotential within this model does not change with pH. The high overpotential on Au(100) is due to weak adsorption of $*O_2H$. This calculation fails to explain the observed exceptional ORR activity of Au(100) in alkaline media. The failure of the CHE method is due to limitations of a simple metal/vacuum model at zero charge to represent a charged

Received: March 5, 2019
Revised: May 1, 2019
Published: May 7, 2019

DOI: 10.1021/acscatal.9b00955
ACS Catal. 2019, 9, 5567−5573

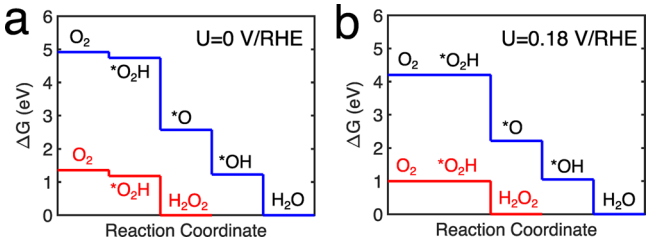

Figure 1. Free energy diagrams of the ORR on Au(100) at applied potentials (a) $U = 0$ and (b) $U = 0.18$/RHE. The $4e^-$ and $2e^-$ pathways are shown with blue and red lines, respectively.

electrochemical interface normally operating at constant potential conditions. In addition to the chemisorption of reaction intermediates, the free energy of a reaction at an electrochemical interface should also include the interaction between adsorbates and the electric field within the electric double layer (EDL).[13] Additionally, adsorbates can significantly modify the capacitance and the potential of zero charge (PZC) of the interface, thus leading to differences in surface charge density for bare vs adsorbed interfaces under constant potential conditions. This grand-canonical contribution is a result of a change in surface charge density upon adsorption and has been found to be prominent for calculating adsorption energies under constant potential conditions.[14−16] Above all, the adsorption and reaction energies are dependent on the applied potential. In order to take these effects into consideration and evaluate the potential-dependent adsorption energies, we combine the double reference method with continuum implicit solvation model to simulate the EDL at the electrode/electrolyte interface under constant potential conditions.

The pH can also affect the adsorption energies of reaction intermediates by effectively changing the electric potential. Indeed, by changing the pH value, the electric potential on the standard hydrogen electrode (SHE) scale also changes at a fixed potential on the RHE scale according to the relation

$$U_{\mathrm{RHE}} = U_{\mathrm{SHE}} + k_{\mathrm{B}}T\ \ln(10)\mathrm{pH}/e \tag{1}$$

For example, if U_{RHE} is held at 1 V, the values of U_{SHE} are 1.0 V and 0.17 V at pH = 0 and pH = 14, respectively. This difference in U_{SHE} then leads to different strengths of the electric field in the EDL, assuming the width of the EDL remains constant, and different surface charges in acid and base solutions.

In this study, we used DFT calculations, considering solvation, potential, and pH effects, to provide insight into the exceptional ORR activity on the Au(100) surface in base. Based on our DFT-calculated reaction energetics, we found that two dominant factors explain the puzzling ORR activity on Au(100). First, oxygenated species bind more strongly on Au(100) in base. Second, adsorbed OH can further stabilize oxygenated species, including $*O_2H$.

COMPUTATIONAL METHODS

DFT calculations with a plane-wave basis set were performed using the Vienna *Ab initio* Simulation Package.[17−19] The generalized gradient approximation functional of the Perdew−Wang 91[20] form was used to describe the electronic exchange and correlation energy. Electron−ion interactions were treated with ultrasoft pseudopotentials.[21] In all calculations, the energy cutoff of the plane wave basis set was 400 eV. The Brillouin zone was sampled using the Monkhorst−Pack scheme[22] with a $2 \times 2 \times 1$ k-point mesh for the $p(4 \times 4)$ Au(100) surface slab. For smaller $p(2 \times 2)$ Au(100) surface slab, a $4 \times 4 \times 1$ k-point mesh was used. Optimized structures were obtained by minimizing the forces on each ion until they fell below 0.05 eV/Å. All calculations are nonspin-polarized; all reaction intermediates are assumed to be closed-shell.

Slab models were employed to simulate clean and adsorbate-covered Au(100) surfaces. The slab models consisted of five Au layers. The Au atoms in the middle layer were fixed during structural relaxation. Symmetric slabs had adsorbates on both surfaces, separated by a 20 Å vacuum layer, in order to eliminate the electric dipole between periodic images. The lattice constant of Au was calculated to be 4.183 Å. The use of an unreconstructed Au(100) surface is reasonable because experimentally the hexagonal reconstruction can only be induced at a potential of −0.4 V/SCE (−0.16 V/SHE)[23] and the reconstruction is restored at a potential of 0.36 V/SCE (0.6 V/SHE).[24] DFT calculations also qualitatively predicted that the unreconstructed surface is stable when the applied potential is sufficiently positive.[25] Hence, in the normal potential range of ORR, the unreconstructed surface should be stable.

We employed the double-reference method to model the electrochemical metal/solution interface and to evaluate the influence of solvation and the applied potential on the reaction energetics.[26,27] The aqueous environment in this study is modeled as a continuum dielectric as implemented by the Hennig group in the VASPsol code[28,29] with the relative permittivity of the electrolyte set to 80. Details of the double reference method can be found in refs 26 and 27. Briefly, the EDL at the metal/aqueous interface is simulated by varying the number of electrons of the system. A uniform background of compensating counter charge is added to maintain charge neutrality of the supercell. The charged slab together with the compensating background charge polarize the electrolyte near the metal/solution interface, creating an electrostatic potential profile that simulates the EDL. The electric potential of the slab referenced to the SHE is calculated as

$$U_q\ (\mathrm{V/SHE}) = -4.6 - \phi_q(f)/\mathrm{eV} \tag{2}$$

where $-\phi_q(f)$ is the work function of the charged slab in aqueous solution and 4.6 V is the work function of the H_2/H^+ couple at standard conditions. Actually, the work function of SHE measurement is scattered from 4.4 through 4.8 V;[30] we took the average value of 4.6 V for our calculations. The total energy of the charged system is then corrected for the interaction with the background charge as well as for the difference in the number of electrons in the system by

$$E_{\mathrm{correction}} = \int_0^q \langle \overline{V_{\mathrm{tot}}} \rangle\ \mathrm{d}Q + qU_q \tag{3}$$

For each structure, calculations are performed at charges of −3.2e to +3.2e with steps of +0.8e. The total free energy at the 11 charge values is then fit to a quadratic function to provide the free energy as a continuous function of potential. The quadratic form is consistent with a capacitor created by the charged-slab/background-charge system, which takes the form

$$E(U) = -\frac{1}{2}C(U - U_0)^2 + E_0 \tag{4}$$

DOI: 10.1021/acscatal.9b00955
ACS Catal. 2019, 9, 5567−5573

where U_0 refers to the potential of zero charge (PZC), E_0 is the energy at the PZC, and C is the capacitance of the surface. From the fitted quadratic functions for the bare slab and slabs with adsorbates, the binding energies and reaction energetics as a function of electric potential are calculated.

The energetics of the electrochemical ORR was calculated with the CHE method.[3,31] Briefly, the Gibbs free energy change of each electrochemical elementary step of the ORR was calculated with DFT. The $4e^-$ ORR reaction mechanism was assumed to follow the four-step associative mechanism represented by

$$O_2(g) + H^+ + e^- \leftrightarrow {}^*O_2H \quad (5)$$

$${}^*O_2H + H^+ + e^- \leftrightarrow {}^*O + H_2O(l) \quad (6)$$

$${}^*O + H^+ + e^- \leftrightarrow {}^*OH \quad (7)$$

$${}^*OH + H^+ + e^- \leftrightarrow H_2O(l) \quad (8)$$

The $2e^-$ reaction pathway producing H_2O_2 is

$$O_2(g) + H^+ + e^- \leftrightarrow {}^*O_2H \quad (9)$$

$${}^*O_2H + H^+ + e^- \leftrightarrow H_2O_2(l) \quad (10)$$

The free energy change of each elementary step is calculated as $\Delta G = \Delta E - T\Delta S + \Delta ZPE$, where ΔZPE is the change in zero-point energy. The energy of these elementary steps (ΔE) are the energy differences between the DFT-calculated energies of the product and reactant states. In this work, ΔE, as calculated from the double reference method, is potential-dependent. The chemical potential of the solvated proton and electron pair (H^++e^-) at standard conditions (pH = 0, T = 298.15 K) is calculated as $1/2G_{H2} + eU_{SHE}$ assuming equilibrium at the standard hydrogen electrode. The changes in ΔZPE and $T\Delta S$ are calculated using previously determined values.[3] For the $4e^-$ and $2e^-$ pathways, the equilibrium potentials at standard conditions are 1.23 and 0.68 V/SHE, respectively. The CHE method is also used to construct the surface Pourbaix diagram of Au(100) in aqueous solution.[31]

RESULTS AND DISCUSSION

Potential-Dependent Adsorption Energies of Oxygenated Species on Au(100). The calculated total energies of the bare Au(100)/aqueous interface and the interface with adsorbed oxygenated species ($*O_2H$, *O, and *OH) as a function of U/SHE are shown in Figure 2a. The parameters of the quadratic potential-dependent total energies are included in Table 1. The adsorption energies of the oxygenated species are shown in Figure 2b. All oxygenated species are found to be most stable at the bridge site on Au(100). The atomic structures of bare Au(100) slabs and with adsorbates are shown in Figure 2c.

First, it can be seen that the calculated 0.52 V PZC of Au(100) is consistent with the experimental value of 0.53 V as measured in 0.1 M $HClO_4$.[32] After adsorption of $*O_2H$ at the Au(100)/aqueous interface, the PZC has shifted to 0.71 V and the capacitance of the interface changes from 4.33 to 4.83 e/V. The PZC shift can be attributed to the electron-withdrawing effect of $*O_2H$ from the metal surface, which increases its work function and thus increases the PZC. Including these two effects, the $*O_2H$ adsorption energy increases with applied potential because the $*O_2H$ adsorbed interface is charged with more electrons at the same potential as compared to the bare

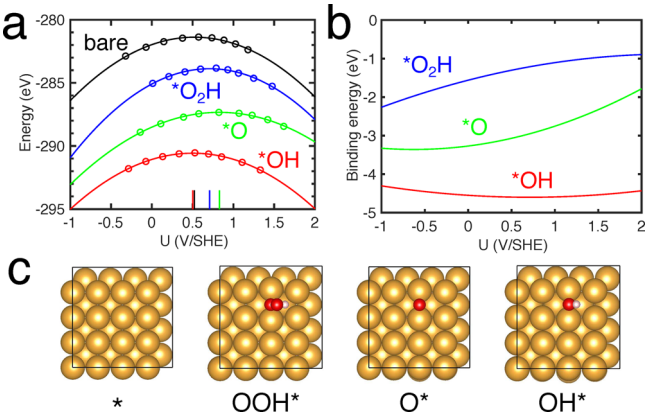

Figure 2. (a) Total energies of clean Au(100) (black), $*O_2H$/Au(100) (blue), *O/Au(100) (green), and *OH/Au(100) (red) as a function of applied potential U. The calculated total energies are shown as circles, and polynomial fits to these energies are the solid lines. (b) Adsorption energies of $*O_2H$ (blue), *O (green), and *OH (red) as a function of U. (c) Atomic models of Au(100), $*O_2H$/Au(100), *O/Au(100), and *OH/Au(100).

Table 1. Fitted Parameters of the Quadratic Equation for Calculating the Total Energies of Various Models

model	U_0 (V/SHE)	C (e/V)	E_0 (eV)
Au(100)	0.52	4.34	−234.75
Au(100) + OOH*	0.71	4.83	−263.63
Au(100) + O*	0.83	3.42	−245.34
Au(100) + OH*	0.50	3.93	−255.32
Au(100) + OH*	0.50	3.93	−255.32
Au (100) + OH* + OOH*	0.86	5.03	−284.13
Au(100) + OH* + O*	0.98	3.66	−265.71
Au(100) + OH* + OH*	0.60	3.92	−276.00

interface. The adsorption of *O also shifts the PZC from 0.52 to 0.83 V and decreases the capacitance from 4.33 to 3.93 e/V. As a result of these two effects, the adsorption energy of *O increases more quickly with increasing applied potential. The adsorption energy of *OH remains roughly constant with respect to the applied potential because the PZC does not shift significantly upon *OH adsorption; the slight decrease in capacitance results in slightly increased binding energies when the applied potential shifts from the PZC of the interface.

The pH value can affect the adsorption energies of the oxygenated species by changing the effective electric potential according to eq 1, as shown schematically in Figure 3a. The case exhibited in the figure resembles the adsorption of $*O_2H$

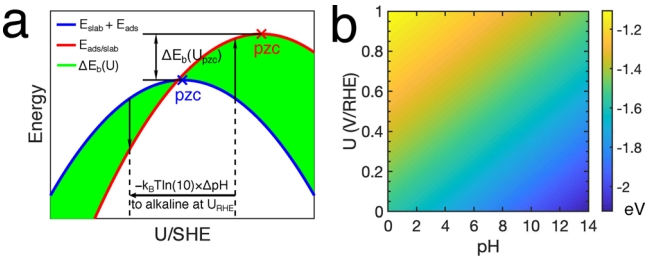

Figure 3. (a) Schematic plot of potential- and pH-dependent adsorption energy. (b) Potential- and pH-dependent adsorption energy of $*O_2H$ on Au(001).

DOI: 10.1021/acscatal.9b00955
ACS Catal. 2019, 9, 5567−5573

in the sense that adsorption results in an upshift of the PZC. Consequently, the adsorption energy (green shaded area) also increases with respect to the potential (U_SHE). According to eq 1, the electric potential (U_SHE) would shift by k_BT ln 10 × ΔpH when the pH value varies by ΔpH. In the specific case shown, the adsorption energy decreases as pH value increases; that is, adsorption energy increases as the electrolyte is changed from acid to base. This is also the case for $*O_2H$. Figure 3b shows the adsorption energy of $*O_2H$ on Au(100) as a function of applied potential (U_RHE) and the pH. We can see that the adsorption energy of $*O_2H$ decreases as the pH increases.

pH-Dependent ORR Activity and Reaction Pathway on Au(100). We expect that the ORR overpotential on Au(100) also depends on the pH value as a result of the pH-dependent adsorption energies. We assessed the onset potentials of the ORR on Au(100) at different pH values as shown in Figure 4. The ORR onset potential at pH = 1 is calculated to be 0.36 V/RHE. The potential determining step is $*O_2H$ formation because of its relatively low adsorption strength on Au(100). The $4e^-$ and $2e^-$ mechanisms share the same onset potential and potential determining step. The reaction pathway for oxygen reduction depends on the relative reaction rates of H_2O_2 formation vs *O formation, which is not addressed in the current study. The onset potential is increased to 0.61 V/RHE when the pH is 13. The improved ORR activity in alkaline solution is due to the stabilization of $*O_2H$ on Au(100). The results provide insights on the pH-dependent ORR activity on Au(100), which is attributed to the potential-dependent adsorption of $*O_2H$. This predicted onset potential is more accurate than the CHE method using gas-phase adsorption energies. However, the predicted onset potential is still less positive than the experimental value of 0.8 V/RHE.

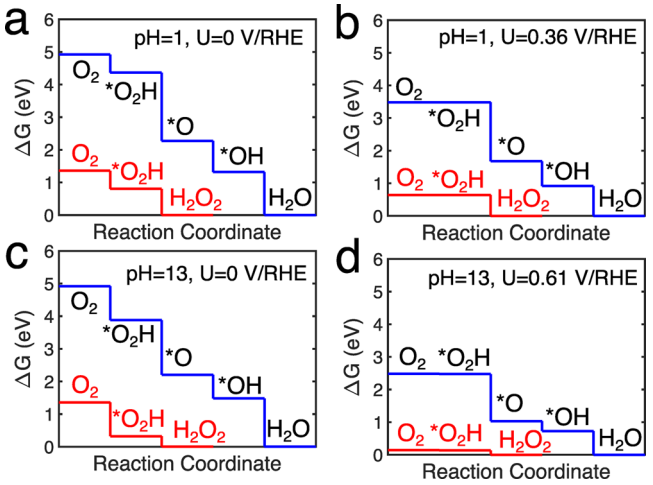

Figure 4. Free energy diagrams of the ORR on Au(100) at (a) $U = 0$ V/RHE, pH = 1, (b) $U = 0.36$ V/RHE, pH = 1, (c) $U = 0$ V/RHE, pH = 13, and (d) $U = 0.61$ V/RHE, pH = 13. The $4e^-$ and $2e^-$ pathways are presented with blue and red lines, respectively.

Influence of Adsorbed OH* on the ORR Activity and Reaction Pathway on Au(100). Experiments have shown that the adsorption of *OH is important for the high ORR activity of Au(100) in alkaline media. Accordingly, we examined the influence of an adsorbed *OH on the ORR activity of an adjacent site on Au(100). The proposed atomic models and the adsorption energies of oxygenated species on the *OH precovered Au(100) surface are presented in Figure 5. The quadratic equations of the fit to the potential-dependent total energies are included in Table 1. We can see that the shifts in PZC and capacitance upon adsorption have the same trend as is the case of adsorption on the clean Au(100) surface. However, the magnitude of the PZC shifts on the *OH-precovered Au(100) are greater than on the clean Au(100). For example, after $*O_2H$ adsorption on the *OH-precovered Au(100), the PZC changes from 0.5 to 0.86 V/SHE; the 0.36 V shift is 0.16 V larger than that on the clean Au(100) surface. The increased shifts of PZC are similar in the case of *O and *OH. The adsorption energies of the oxygenated species increase more rapidly as the applied potential increases. Hence, by increasing the pH values—which decreases U/SHE when U/RHE is fixed—the $*O_2H$ is further stabilized, leading to improved ORR activity.

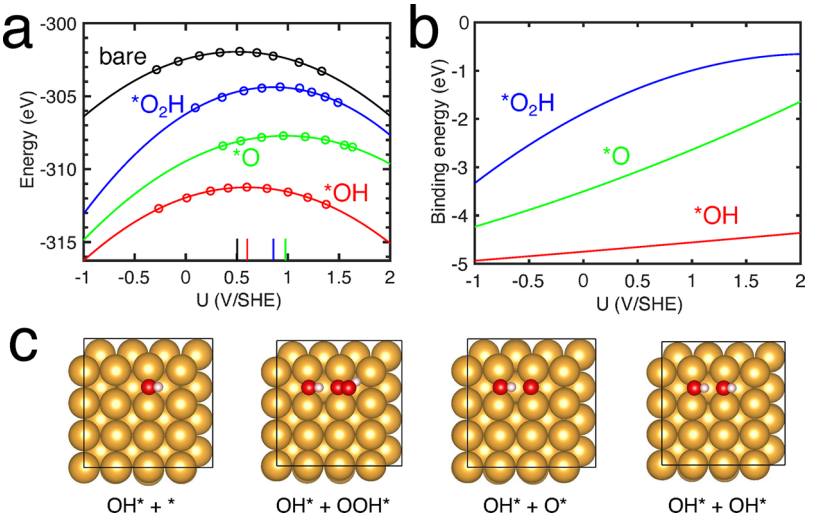

Figure 5. (a) Total energies of the *OH/Au(100) (black), *OH + $*O_2H$/Au(100) (blue), *OH+*O/Au(100) (green), and *OH+*OH/Au(100) (red) as a function of applied potential U. The calculated total energies are shown as circles, and polynomial fits to these energies are the solid lines. (b) Adsorption energies of $*O_2H$ (blue), *O (green), and *OH (red) as a function of U on the *OH precovered Au(100) surface. (c) Atomic models of *OH/Au(100), *OH+$*O_2H$/Au(100), *OH+*O/Au(100), and *OH+*OH/Au(100).

DOI: 10.1021/acscatal.9b00955
ACS Catal. 2019, 9, 5567−5573

The ORR activity on the *OH-precovered Au(100) is determined from our calculated free energy diagrams in Figure 6. In acidic media (pH = 1), the ORR onset potential is 0.44

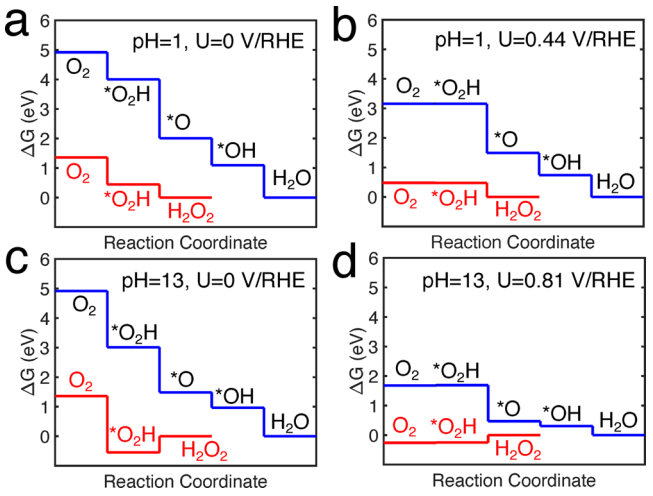

Figure 6. Free energy diagrams of the ORR on Au(100) at (a) U = 0 V/RHE, pH = 1, (b) U = 0.44 V/RHE, pH = 1, (c) U = 0 V/RHE, pH = 13, and (d) U = 0.81 V/RHE, pH = 13. The 4e$^-$ and 2e$^-$ pathways are presented with blue and red lines, respectively.

V/RHE. Both the 2e$^-$ and 4e$^-$ reaction pathways are thermodynamically active. In alkaline media (pH = 13), the onset potential increases to 0.81 V/RHE due to *O_2H stabilization. More importantly, *O_2H adsorption is sufficiently strong so that the production of H_2O_2 is unfavorable and only the 4e$^-$ pathway is active. These results are consistent with the experiment in that the 4e$^-$ reduction is only observed in alkaline media and coincides with *OH adsorption on the Au(100) surface.

Adsorbed *OH primarily influences the reactivity of its neighboring sites. The onset potential of ORR on the next nearest neighbor is only 0.44 V/RHE at pH = 13 (see Figures S1 and S2), which is lower than the 0.61 V/RHE on clean Au(100). We postulate that hydrogen binding between the *OH and the oxygenated species adsorbed at the nearest neighboring site plays an important role in promoting ORR activity. To test this assumption, we considered a model with the hydrogen atom in *OH turned away from the adsorbed oxygenated species. The onset potential at this site is predicted to be 0.66 V/RHE at pH = 13 (see Figures S3 and S4). Thus, the stabilization effect due to hydrogen binding for the oxygenated species, and especially *O_2H, is shown to promote the ORR activity. The predicted 0.66 V/RHE is higher than the 0.61 V/RHE on clean Au(100), so there must be a promoting effect other than hydrogen bonding. We plot the charge density distribution of the surface layer of Au(100) with adsorbed *OH in Figure 7. It can be seen that due to *OH adsorption, electrons are depleted from the neighboring bridge site, causing a favorable electrostatic interaction between the electron-rich oxygenated species and the bridge site. Prieto et al. also proposed that Au(100) is a good catalyst for the ORR because its surface is positively charged at low overpotential so that negatively charged intermediates are attracted to the electrode.[33]

Surface Pourbaix Diagram of Au(100). We have demonstrated that the ORR activity is the highest on Au(100) when there is a *OH neighboring the active site. It

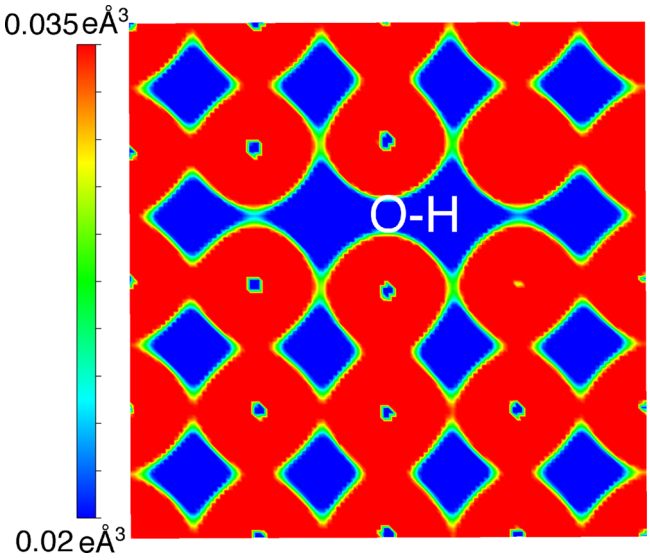

Figure 7. 2D charge density plot of the surface layer of Au(100) with *OH adsorption.

has not yet been shown that this active site is thermodynamically favorable under reaction conditions. Hence, we construct the surface Pourbaix diagram of Au(100) to explore the stable surface phases under reaction conditions, as shown in Figure 8,

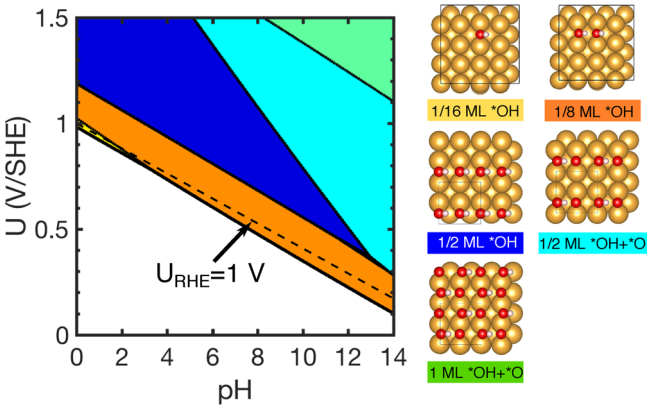

Figure 8. Surface Pourbaix diagram of Au(100) and atomic structures of the stable surface phases.

along with atomic models of the stable surface phases. All surface phases that are included in the diagram construction can be viewed in Figure S5. It can be seen that when pH < 2, single OH^- adsorbs on Au(100) when U_{RHE} equals to 1 V. When pH > 2, OH^- adsorption at lower U_{RHE} is facile because of stronger *OH adsorption. More importantly, *OH adsorbs on Au(100) in pairs with neighboring *OH. Specifically, at pH = 13, *OH adsorption occurs at U_{RHE} = 0.93 V. This predicted value is consistent with the hydroxyl adsorption peak observed in the cyclic voltammetry on Au(100).

Under ORR reaction conditions, isolated *OH forms at potentials higher than 0.61 V/RHE at pH = 13 (see Figure 4d). When *OH is present, the dually adsorbed *OH forms due to its higher stability at potentials over 0.61 V/RHE at pH = 13. Consequently, in the potential window of 0.61 to 0.81 V/RHE, the 4e$^-$ ORR is facile because the *OH modified active site becomes accessible. It should be noted that in this potential range, adsorbed *OH and other oxygenated species

DOI: 10.1021/acscatal.9b00955
ACS Catal. 2019, 9, 5567−5573

can still be reduced, since dual *OH binding is only stable above 0.93 V/RHE in an oxygen-free environment. Consequently, for ORR, the optimal active site is both dynamically formed and annihilated.

Surface Structure Effects: Comparison between Au(100), Au(111), and Au(110). The ORR activity in alkaline solution on Au is strongly sensitive to surface structure. Au(100) has a much higher ORR activity than those of Au(111) and Au(110) in alkaline solution.[34] To explain these surface structure effects, we conducted calculations of binding energies of ORR intermediates on the Au(111) and Au(110) surfaces.

The results of Au(111) are shown in Figure S6 and Figure S7. The parameters of the quadratic potential-dependent total energies are included in Table S2. For simplicity, we focus on the binding energy of $*O_2H$ since $*O_2H$ stabilization is the overpotential determining factor, as can be seen from the case of Au(100). The binding energy of $*O_2H$ is relatively constant as a function of applied potential because the PZC shift before and after $*O_2H$ adsorption is small. As a result, the ORR activity on Au(111) is relatively insensitive to pH. The ORR activity on Au(111) in alkaline solution is much lower than on Au(100) because the $*O_2H$ binding energy on Au(111) is much higher at low applied potentials than that on Au(100). From the point of view of surface structure, the close-packed Au(111) surface interacts weakly with the $*O_2H$ and thus less electron density is transferred from the Au to the adsorbate, resulting in a small PZC shift. Indeed, a Bader analysis shows that the $*O_2H$ adsorbate on Au(111) has a charge of 1.47 e, while on Au(100) it has a charge of 1.51 e.

The calculated results for clean Au(110) are shown in Figures S8 and S9. The parameters of the quadratic potential-dependent total energies are included in Table S2. The surface structure of Au(110) is similar to that of Au(100) except that the spacing between the Au rows is elongated in one direction. The $*O_2H$ adsorption is also adsorbed at the Au bridge site giving a similar binding energy of $*O_2H$ to that on the Au(100). Consequently, the ORR activities on clean Au(110) and Au(100) are similar. In contrast to the Au(100) surface, the *OH binding on Au(110) has a very limited promotional effect on the ORR activity at an adjacent site, as a result of the longer distance between the Au rows. The results of calculated binding energies and ORR activities on *OH/Au(110) can be found in Figures S10 and S11. It can be seen that *OH only promotes the onset potential from 0.65 V/RHE to 0.73 V/RHE at pH = 13 on Au(110).

CONCLUSION

We have shown that the potential- and pH-dependent adsorption energies of ORR intermediates are essential for understanding the high ORR activity of Au(100) in alkaline media. In acidic media, $*O_2H$ adsorption is too weak on Au(100) for the ORR. In alkaline media, the ORR operates at a lower U_{SHE} as compared to an acidic solution, which results in stabilization of $*O_2H$ adsorption due to enhanced electron transfer to $*O_2H$; thus, ORR activity is promoted. Further, chemisorbed *OH promotes electron transfer to $*O_2H$ because of hydrogen binding between *OH and $*O_2H$ and electron depletion in the neighborhood of *OH. Due to the influence of *OH, the onset potential of ORR is 0.81 V/RHE. More importantly, at this potential, only the $4e^-$ reduction pathway is kinetically favorable. A surface Pourbaix diagram analysis shows that a pair of neighboring *OH is more stable than single *OH, especially in alkaline conditions. The catalytic trends of the ORR on Au(100) observed in previous experiments are explained by the calculations in this study.

ASSOCIATED CONTENT

Supporting Information

The Supporting Information is available free of charge on the ACS Publications website at DOI: 10.1021/acscatal.9b00955.

Fitted parameters of the quadratic equation and free energy diagrams (PDF)

AUTHOR INFORMATION

Corresponding Author

*E-mail: henkelman@utexas.edu.

ORCID

Graeme Henkelman: 0000-0002-0336-7153

Notes

The authors declare no competing financial interest.

ACKNOWLEDGMENTS

This work is supported by the Department of Energy under contract DE-SC0010576 and the Welch Foundation under grant F-1841. The calculations were done at the National Energy Research Scientific Computing Center and the Texas Advanced Computing Center.

REFERENCES

(1) Stamenkovic, V. R.; Fowler, B.; Mun, B. S.; Wang, G.; Ross, P. N.; Lucas, C. A.; Marković, N. M. Improved Oxygen Reduction Activity on $Pt_3Ni(111)$ via Increased Surface Site Availability. *Science* **2007**, *315*, 493−497.

(2) Stamenkovic, V. R.; Mun, B. S.; Arenz, M.; Mayrhofer, K. J.; Lucas, C. A.; Wang, G.; Ross, P. N.; Markovic, N. M. Trends in Electrocatalysis on Extended and Nanoscale Pt-Bimetallic Alloy Surfaces. *Nat. Mater.* **2007**, *6*, 241−247.

(3) Nørskov, J. K.; Rossmeisl, J.; Logadottir, A.; Lindqvist, L.; Kitchin, J. R.; Bligaard, T.; Jónsson, H. Origin of the Overpotential for Oxygen Reduction at a Fuel-Cell Cathode. *J. Phys. Chem. B* **2004**, *108*, 17886−17892.

(4) Zurilla, R. W.; Sen, R. K.; Yeager, E. The Kinetics of the Oxygen Reduction Reaction on Gold in Alkaline Solution. *J. Electrochem. Soc.* **1978**, *125*, 1103−1109.

(5) Adić, R.; Marković, N.; Vešović, V. Structural effects in electrocatalysis: Oxygen reduction on the Au (100) single crystal electrode. *J. Electroanal. Chem. Interfacial Electrochem.* **1984**, *165*, 105−120.

(6) Štrbac, S.; Anastasijević, N.; Adžić, R. Oxygen Reduction on Au (100) and Vicinal Au (910) and Au (11,1,1) Faces in Alkaline Solution: A Rotating Disc-Ring Study. *J. Electroanal. Chem.* **1992**, *323*, 179−195.

(7) Štrbac, S.; Adšić, R. The Influence of pH on Reaction Pathways for O_2 Reduction on the Au(100) Face. *Electrochim. Acta* **1996**, *41*, 2903−2908.

(8) Štrbac, S.; Adžić, R. The Influence of OH^- Chemisorption on the Catalytic Properties of Gold Single Crystal Surfaces for Oxygen Reduction in Alkaline Solutions. *J. Electroanal. Chem.* **1996**, *403*, 169−181.

(9) Shao, M. H.; Adzic, R. R. Spectroscopic Identification of the Reaction Intermediates in Oxygen Reduction on Gold in Alkaline Solutions. *J. Phys. Chem. B* **2005**, *109*, 16563−16566.

(10) Mei, D.; He, Z. D.; Zheng, Y. L.; Jiang, D. C.; Chen, Y.-X. Mechanistic and Kinetic Implications on the ORR on a Au(100) Electrode: pH, Temperature and H-D Kinetic Isotope Effects. *Phys. Chem. Chem. Phys.* **2014**, *16*, 13762−13773.

DOI: 10.1021/acscatal.9b00955
ACS Catal. 2019, 9, 5567−5573

(11) Stamenkovic, V. R.; Strmcnik, D.; Lopes, P. P.; Markovic, N. M. Energy and Fuels from Electrochemical Interfaces. *Nat. Mater.* **2017**, *16*, 57−69.
(12) Lu, F.; Zhang, Y.; Liu, S.; Lu, D.; Su, D.; Liu, M.; Zhang, Y.; Liu, P.; Wang, J. X.; Adzic, R. R.; Gang, O. Surface Proton Transfer Promotes Four-Electron Oxygen Reduction on Gold Nanocrystal Surfaces in Alkaline Solution. *J. Am. Chem. Soc.* **2017**, *139*, 7310−7317.
(13) Rossmeisl, J.; Nørskov, J. K.; Taylor, C. D.; Janik, M. J.; Neurock, M. Calculated Phase Diagrams for the Electrochemical Oxidation and Reduction of Water over Pt(111). *J. Phys. Chem. B* **2006**, *110*, 21833−21839.
(14) Steinmann, S. N.; Michel, C.; Schwiedernoch, R.; Sautet, P. Impacts of Electrode Potentials and Solvents on the Electroreduction of CO_2: a Comparison of Theoretical Approaches. *Phys. Chem. Chem. Phys.* **2015**, *17*, 13949−13963.
(15) Kim, D.; Shi, J.; Liu, Y. Substantial Impact of Charge on Electrochemical Reactions of Two-Dimensional Materials. *J. Am. Chem. Soc.* **2018**, *140*, 9127−9131.
(16) Duan, Z.; Henkelman, G. Calculations of the pH-Dependent Onset Potential for CO Electrooxidation on Au(111). *Langmuir* **2018**, *34*, 15268−15275.
(17) Kresse, G.; Hafner, J. Ab Initio Molecular Dynamics for Liquid Metals. *Phys. Rev. B: Condens. Matter Mater. Phys.* **1993**, *47*, 558.
(18) Kresse, G.; Furthmüller, J. Efficiency of Ab-Initio Total Energy Calculations for Metals and Semiconductors Using a Plane-Wave Basis Set. *Comput. Mater. Sci.* **1996**, *6*, 15−50.
(19) Kresse, G.; Furthmüller, J. Efficient Iterative Schemes for Ab Initio Total-Energy Calculations Using a Plane-Wave Basis Set. *Phys. Rev. B: Condens. Matter Mater. Phys.* **1996**, *54*, 11169.
(20) Perdew, J. P.; Wang, Y. Accurate and Simple Analytic Representation of the Electron-Gas Correlation Energy. *Phys. Rev. B: Condens. Matter Mater. Phys.* **1992**, *45*, 13244.
(21) Kresse, G.; Joubert, D. From Ultrasoft Pseudopotentials to the Projector Augmented-Wave Method. *Phys. Rev. B: Condens. Matter Mater. Phys.* **1999**, *59*, 1758−1775.
(22) Monkhorst, H. J.; Pack, J. D. Special Points for Brillouin-Zone Integrations. *Phys. Rev. B* **1976**, *13*, 5188−5192.
(23) Schneider, J.; Kolb, D. M. Potential-Induced Surface Reconstruction of Au(100). *Surf. Sci.* **1988**, *193*, 579−592.
(24) Striegler, H.; Skoluda, P.; Kolb, D. M. On the Stability of Unreconstructed Au(100)-(1 × 1) at Negative Potentials in Aqueous Sulfate Solution. *J. Electroanal. Chem.* **1999**, *471*, 9−13.
(25) Jacob, T. Potential-Induced Lifting of the Au(100)-Surface Reconstruction Studied with DFT. *Electrochim. Acta* **2007**, *52*, 2229−2235.
(26) Taylor, C. D.; Wasileski, S. A.; Filhol, J.-S.; Neurock, M. First Principles Reaction Modeling of the Electrochemical Interface: Consideration and Calculation of a Tunable Surface Potential from Atomic and Electronic Structure. *Phys. Rev. B: Condens. Matter Mater. Phys.* **2006**, *73*, 165402.
(27) Filhol, J.-S.; Neurock, M. Elucidation of the Electrochemical Activation of Water over Pd by First Principles. *Angew. Chem., Int. Ed.* **2006**, *45*, 402−406.
(28) Mathew, K.; Sundararaman, R.; Letchworth-Weaver, K.; Arias, T. A.; Hennig, R. G. Implicit Solvation Model for Density-Functional Study of Nanocrystal Surfaces and Reaction Pathways. *J. Chem. Phys.* **2014**, *140*, 084106.
(29) Fishman, M.; Zhuang, H. L.; Mathew, K.; Dirschka, W.; Hennig, R. G. Accuracy of Exchange-Correlation Functionals and Effect of Solvation on the Surface Energy of Copper. *Phys. Rev. B: Condens. Matter Mater. Phys.* **2013**, *87*, 245402.
(30) Trasatti, S. Structure of the Metal/Electrolyte Solution Interface: New Data for Theory. *Electrochim. Acta* **1991**, *36*, 1659−1667.
(31) Hansen, H. A.; Rossmeisl, J.; Nørskov, J. K. Surface Pourbaix Diagrams and Oxygen Reduction Activity of Pt, Ag and Ni(111) Surfaces Studied by DFT. *Phys. Chem. Chem. Phys.* **2008**, *10*, 3722.
(32) Hamm, U.; Kramer, D.; Zhai, R.; Kolb, D. The PZC of Au(111) and Pt(111) in a Perchloric Acid Solution: an Ex Situ Approach to the Immersion Technique. *J. Electroanal. Chem.* **1996**, *414*, 85−89.
(33) Prieto, A.; Hernández, J.; Herrero, E.; Feliu, J. M. The Role of Anions in Oxygen Reduction in Neutral and Basic Media on Gold Single-Crystal Electrodes. *J. Solid State Electrochem.* **2003**, *7*, 599−606.
(34) Schmidt, T.; Stamenkovic, V.; Arenz, M.; Markovic, N.; Ross, P. Oxygen Electrocatalysis in Alkaline Electrolyte: Pt(hkl), Au(hkl) and the Effect of Pd-Modification. *Electrochim. Acta* **2002**, *47*, 3765−3776.

DOI: 10.1021/acscatal.9b00955
ACS Catal. 2019, 9, 5567−5573